Sustainable Energy & Fuels

ROYAL SOCIETY OF CHEMISTRY

PAPER

View Article Online
View Journal | View Issue

Cite this: *Sustainable Energy Fuels*, 2023, 7, 2087

A self-assembled molecularly triboelectronegative cellulose nanofiber material with ultrahigh contact triboelectrification for the design of green triboelectric nanogenerators†

Yang Li,[a] Nannan Wang,*[c] Sheng Wang,[c] Bofan Li,[c] Enyi Ye,[bc] Xianjun Loh[bc] and Zibiao Li*[bcd]

The research and development of bio-based electronegative tribolayers will accelerate the further application of green triboelectric nanogenerators (G-TENGs), which is beneficial to alleviate the environmental pollution caused by the non-recyclability of traditional TENGs. Herein, we prepared a cellulose nanofiber (CNF) based triboelectronegative tribolayer material with ultrahigh triboelectric charge density, which is obtained by molecular self-assembly of 3-(triethoxysilyl) propionitrile (TESPN) on the surface of a CNF film. Due to the strong electron-withdrawing effect of cyano-groups, the modified CNF film tends to gain electrons and be negatively charged during the triboelectrification process. The results show that the CNF-TESPN@CNF-based green TENG can deliver a current of 14.4 μA and a voltage of 251 V. Moreover, compared to electronegative cellulose acetate, the triboelectric charge density (TECD) of the modified CNF film was increased by 95%, showing ultrahigh contact electrification performance. The smart self-powered system can be used as a wearable device for an energy harvester or corrosion protection of metal surfaces in the ocean.

Received 12th December 2022
Accepted 25th March 2023

DOI: 10.1039/d2se01715f

rsc.li/sustainable-energy

1 Introduction

In recent years, holding remarkable application potential to bring about revolution to our way of life, rapidly increasing research progress has been made in the field of wearable electronics.[1–5] It is highly desirable for exploring technologies to convert ubiquitous mechanical energy in our living environment such as human motion, mechanical triggering and rotation into electricity which can then be utilized to power nanodevices without using a battery.[6–10] However, the triboelectronegative tribolayers of traditional TENGs are usually made of polymer materials such as polytetrafluoroethylene (PTFE), polydimethylsiloxane (PDMS), polystyrene (PS) and other non-degradable materials, which increases the risk of environmental pollution.[11–15] In order to solve this problem, researchers are committed to developing new bio-based tribolayer materials including starch, cellulose, sodium alginate, and silk protein to replace traditional polymer materials.[16–20]

To a certain extent, the special characteristics of these materials, such as abundant sources, simple preparation, degradability, and moisture resistance, have made outstanding contributions to the development of green TENGs.[21–24] However, since cellulose acetate is the most widely used bio-based electronegative tribolayer material currently known, the selectivity of the electronegative tribolayer material for these green TENG devices is relatively single. Furthermore, due to the large crystallinity and the difficulty of modification, the triboelectric charge density of cellulose acetate is low, which seriously affects the further application of green TENGs.[25–27] In order to improve the electrical output of green TENGs, researchers have chemically modified, doped, compounded or patterned the bio-based tribolayer to improve the triboelectric performance.[28,29] Bio-based materials tend to lose electrons in the process of triboelectrification to become positively charged due to rich hydrocarbon groups, so materials such as starch and cellulose are in the electropositive position in the triboelectric sequence.[30,31] Based on this, the modification of bio-based materials only increases the triboelectric charge density of the electropositive tribolayer of TENGs while ignoring the electronegative tribolayer. Therefore, the development of novel bio-based electronegative tribolayers is significant and challenging.

[a]*Blood Transfusion Department, Zhongnan Hospital of Wuhan University, Wuhan 430071, China. E-mail: Liyang0909@whu.edu.cn*

[b]*Institute of Materials Research and Engineering (IMRE), A*STAR (Agency for Science, Technology and Re-search), 2 Fusionopolis Way, Innovis, #08-03, Singapore 138634, Singapore. E-mail: lizb@imre.a-star.edu.sg*

[c]*Institute of Sustainability for Chemicals, Energy and Environment (ISCE2), A*STAR, 2 Fusionopolis Way, Innovis, #08-03, Singapore 627833, Singapore. E-mail: wang_nannan@imre.a-star.edu.sg*

[d]*Department of Materials Science and Engineering, National University of Singapore, Singapore 117575, Singapore*

† Electronic supplementary information (ESI) available. See DOI: https://doi.org/10.1039/d2se01715f

In this work, we fabricated a green TENG (G-TENG) consisting of cellulose nanofibers (CNFs) and 3-(triethoxysilyl) propionitrile (TESPN)-modified CNFs. The electronegative tribolayer of this TENG is rich in cyano-groups with an electron-withdrawing effect, which makes the modified CNFs negatively charged during the triboelectrification process. Compared with commonly used cellulose acetate, TESPN@CNF has better contact electrification performance. The results show that compared to electronegative cellulose acetate, the triboelectric charge density (TECD) of the modified CNF film increased from 46.5 μC m^{-2} to 89.4 μC m^{-2}, with an increase of 95%. Moreover, the current and voltage output of the CNF-TESPN@CNF based TENG increased by 97% and 96%, showing the excellent contact electrification performance of TESPN@CNF as an electronegative tribolayer. This bio-based electronegative tribolayer can be used for the preparation of a green TENG, which has potential applications in energy harvesting, wearable flexible electronics, and metal cathodic protection.

2 Experimental section

2.1 Materials

Bleached softwood kraft pulp (BSKP) was obtained from Mudanjiang Hengfeng Paper Co., Ltd, China. The cellulose sample contained an α-cellulose content of about 92%. The viscosity-average molecular weight (Mη) of the cellulose sample was measured to be 12.1 × 104 g mol^{-1} by using a viscometer in cadoxen at 25 °C. Cellulose acetate (CA, average Mw: ~264.23) and 3-(triethoxysilyl) propionitrile (99%) were purchased from Sigma Aldrich. Copper wire and copper tape purchased from a local market.

2.2 Preparation of the TESPN@CNF based electrode

First, the CNF film was soaked in TESPN/aqueous ethanol (1 wt%) solution for 3 hours. The concentration of ethanol aqueous solution is 90%. After drying in a wind box at 80 °C for 2 h, the TESPN was grafted onto the surface. Then, the modified CNF film was attached to a conductive copper electrode and a copper wire on the backside to obtain the modified CNF film tribo-electrode. The dimensions of the electrodes are "4 cm × 4 cm".

2.3 Preparation of the TESPN@CNF based TENG

The pure CNF film was cut into a size of "4 cm × 4 cm", and a copper electrode was attached to the back with a copper wire taken out to prepare a CNF based electrode as the positive electrode of the TENG. The modified CNF based electrode and pure CNF based electrode were combined into a green TENG.

2.4 Characterization

The surface morphology of the cellulose films was characterized using a JEOL JSM-6710F field emission scanning electron microscope (FE-SEM). The morphology and the elemental components of the samples were investigated using a field emission scanning electron microscope (Hitachi SU8020) equipped with an energy dispersive X-ray spectroscope (EDX, IXRF SDD2830–300D). TEM images were obtained using a TECNAI G2 TF20 high-resolution transmission electron microscope at 200 kV operating voltage (FEI, USA). The crystallization of the films was characterized by X-ray diffraction (XRD) θ–2θ scanning with Cu-Kα radiation using a Rigaku TTR diffractometer. The Fourier transform infrared spectroscopy (FTIR) spectra of the cellulose film were recorded on an FTIR spectrometer (Nicolet 6700, Themo Fisher Scientific Inc.) from 4000 to 400 cm^{-1} at a resolution of 4 cm^{-1}. X-ray photoelectron spectroscopy (XPS) spectra were recorded using a Kratos Axis Ultra instrument employing a monochromatic Al Kα source (1486.69 eV), a hemispherical analyser with a hybrid (electrostatic and magnetic) lens system, charge neutralization by filament-generated, magnetically channelled low-energy electrons, and a delay line detector (DLD). The dielectric constant is tested using a Japanese AET high-frequency dielectric constant tester. The test frequency is 103–107 Hz. The real-time charge of the dielectric was measured using a Faraday cup (284 Coulomb counter, ME-284). During the test, the Faraday cup is connected to an electrometer 6517B, and the real-time electrical signal to be tested is obtained on a computer through LabVIEW software. The surface potential of CNF and TESPN@CNF films was tested with a KEYENCE SK-1000. To measure the triboelectrification output performance, a commercial linear mechanical motor was used to drive the cellulose film based TENGs with a contact-separation mode. The output voltage was measured by using a NI PCIe-6259 DAQ card (National Instruments) with a load resistance of 100 MΩ, while the short-circuit current was measured by using an SR570 low-noise current amplifier (Stanford Research System). During the electrical output test of the TENGs, an impact force of 7 N was maintained at a contact-separation distance of 2.5 cm, and the frequency was 5 Hz.

3 Results and discussion

Fig. 1a shows the schematic structure of the green TENG (G-TENG). During the fabrication, TESPN@CNF replaced the

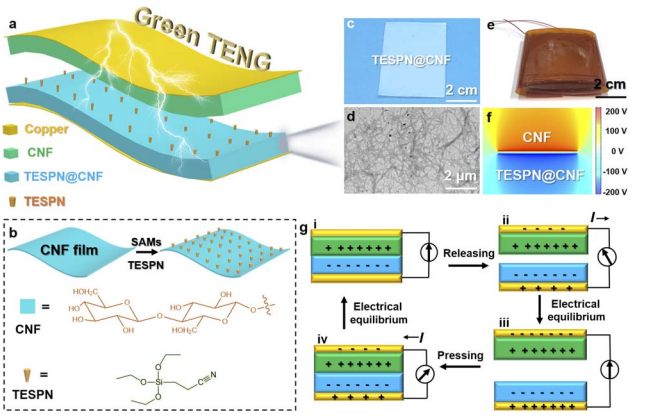

Fig. 1 (a) Schematic diagram of the structure of the green TENG (G-TENG). (b) Preparation process of the TESPN@CNF film. (c) The photo and (d) TEM photo of the TESPN@CNF film. (e) The photo of G-TENG. (f) The potential distribution of G-TENG simulated by COMSOL during the contact electrification. (g) Working mechanism of G-TENG.

traditional electronegative polymer-based tribolayer such as PTFE to ensure the recyclability of the device. TESPN is rich in cyano-groups with an electron-withdrawing effect, which can be used as a "handle" for storing negative charges to keep the modified CNF film electronegativity during the contact electrification process. The preparation process of the TESPN@CNF film is shown in Fig. 1b. The CNF film was immersed in TESPN/ethanol aqueous solution for 3 hours to allow the hydrolysed TESPN molecules to self-assemble on the surface. Then, the TESPN@CNF film was obtained after drying in an oven at 80 °C for 2 h. The molecular self-assembly process of TESPN on the surface of the CNF membrane is shown in Fig. S3.† Fig. 1c shows a photograph of the TESPN@CNF film, illustrating that the modified CNF film is a semi-transparent film. As shown in TEM images (Fig. 1d), the CNF has a high aspect ratio with a high specific surface area (the diameter of fibres is 10–20 nm with a few microns in length, according to previous reports[32]). The photo of G-TENG is shown in Fig. 1e. In order to clearly show the potential distribution of the pure CNF and TESPN@CNF tribolayers during the contact electrification process, finite element simulation (FEM) is performed through COMSOL Multiphysics, as shown in Fig. 1f. The results show that the pure CNF and TESPN@CNF are respectively charged with positive and negative charges with equal and opposite signs during the contact electrification process. The dielectric constants of pure CNF and TESPN@CNF are 1.8 and 2.6.[33]

The working mechanism of the CNF-based TENG is shown in Fig. 1g. TENG's ability to generate triboelectric charge is often attributed to the coupling effect of contact charge and electrostatic induction. When the CNF and TESPN@CNF were pressed together, the pressure bent the modified CNF film into full contact with the pure CNF film, resulting in positive charges on the CNF surface and negative charges on the modified CNF surface (Fig. 1g(i)). When the external pressure was reduced, the CNF partially disengaged from the modified CNF, and the conductive layer generated opposing charges to the tribolayer due to the electrostatic induction effect. Electrons flow from the modified CNF/Cu electrode to the pure CNF/Cu electrode (Fig. 1g(ii)), with the CNF's/Cu layer providing a negative charge and the TESPN@CNF/Cu's layer providing a positive charge. There is no current in the circuit until the CNF and TESPN@CNF are completely separated and the charges have achieved equilibrium (Fig. 1g(iii)). Similarly, when pushed, a reverse current flow from the TESPN@CNF/Cu electrode to the CNF/Cu electrode was recorded (Fig. 1g(iv)). When the TENG experiences contact separation owing to the coupling of contact charged cations and electrostatic induction, current is produced alternately. The TENG test setup is shown in Fig. S1.† Driven by the motor, the two tribolayers of the TENG are continuously contact-separated. The charges generated on the two copper electrodes are transmitted to the current amplifier (SR570) and the NI acquisition card by copper wires, and finally converted into electrical signals on the computer side. The current signal during the TENG working process is shown in Fig. S2.†

To characterize the successful introduction of TESPN, the IR of pure CNF and TESPN@CNF was tested, as shown in Fig. 2a.

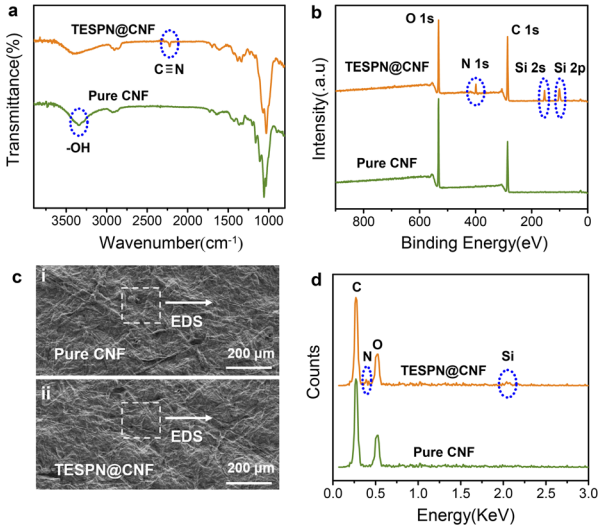

Fig. 2 (a) IR and (b) XPS comparison of pure CNF and TESPN@CNF films. (c) SEM photographs of (i) pure CNF and (ii) TESPN@CNF films. (d) EDS comparison of pure CNF and TESPN@CNF films.

As expected, the absorption peaks of C≡N appear at 2217 cm^{-1} in the IR of modified CNF, which is consistent with a previous report.[34] This outcome demonstrated that TESPN was successfully added to CNF molecules. Then, film surfaces were examined using X-ray photoelectron spectroscopy (XPS) to understand more about the functionalization. Fig. 2b displays the full wavelength survey scan spectra of the pure CNF and modified CNF films. Peaks for O and C, the two components that make up the majority of cellulose, were visible in both films. The TESPN@CNF film showed absorption peaks of N (1s), Si (2s) and Si (2p) at 399.3 eV, 155.3 eV and 99.7 eV, indicating the existence of N and Si elements on the surface. In addition, the atomic content of N and Si on the surface of the CNF film was tested by XPS to characterize the content of TESPN, as shown in Table S1.† The results showed that the atomic contents of N and Si were 1.74% and 1.21%, respectively, indicating that the content of TESPN was 1.21–1.74%. The SEM images of the pure CNF and TESPN@CNF films are shown in Fig. 2c(i) and 2c(ii), illustrating the similar surface morphology of the two films. In addition, the EDS test results of the TESPN@CNF film showed the presence of N and Si elements (Fig. 2d). Subsequently, the ^{13}C-solid-state NMR of the TESPN@CNF film was performed to further characterize the chemical bond structure of TESPN and CNF, as shown in Fig. S4.† The results showed that the chemical shift of CN appeared at 130.5 ppm, which proved the existence of a chemical bond between TESPN and CNF.

Fig. 3 shows the electrical output comparison of cellulose acetate based and TESPN@CNF based TENGs. Using pure CNF as the electropositive tribolayer, the I_{sc} comparison of the two TENGs is shown in Fig. 3a. The results show that when cellulose acetate is used as the electronegative friction layer, the green TENG can obtain a short-circuit current (I_{sc}) of 7.3 μA. However, when TESPN@CNF replaced cellulose acetate, the I_{sc} of the TENG increased to 14.4 μA, which was increased by 97%. This is

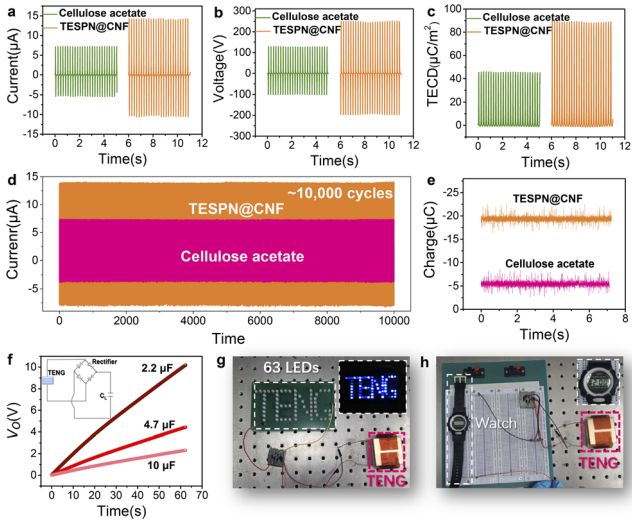

Fig. 3 Comparison of the (a) short-circuit current (I_{sc}), (b) output voltage (V_o), (c) triboelectric charge density (TECD) and (d) stability of cellulose acetate-based and TESPN@CNF-based TENGs. (e) Real-time charges of cellulose acetate and TESPN@CNF films tested by using a Faraday cup. (f) The charging curves of capacitors powered by the TESPN@CNF based TENG. Photos of the demonstration experiment of the TESPN@CNF-based TENG powering (g) 63 LEDs and (h) a watch.

a great improvement and shows the great potential of TESPN@CNF as an electronegative tribological layer for green TENGs. Furthermore, compared with cellulose acetate-based TENGs, the voltage output (V_o) of the TESPN@CNF-based TENG increased by 96% from 128 V to 251 V. The output current (Fig. S5a†) and output voltage (Fig. S5b†) of the TENG were measured under 7 N vertical force to comprehensively evaluate the influence of the frequency. The frequency ranges from 1 Hz to 5 Hz. As a result, the current and voltage show an obvious upward trend as with the increase of the driving frequency, corresponding to the current value of approximately 2.6 μA, 5.3 μA, 9.2 μA, 12.2 μA and 14.4 μA, and the voltage value approximately 32 V, 104 V, 138 V, 187 V and 251 V, respectively. Then, the effect of the external compressive force is also taken into consideration in this study. As can be seen in Fig. S5c and S5d,† when the applied force increases, the output performance also illustrates higher transient current and voltage. The current and voltage under 9 N applied force can reach as high as 16.1 μA and 307 V, approximately 6 times larger than that of 1 N force. However, excessive impact force will accelerate the damage of TENG devices and the distortion of electrical signals. In order to present the experimental results more scientifically, this study chooses a 7 N impact with a frequency of 5 Hz. Then, the triboelectric charge density (TECD) of the two TENGs was calculated to characterize the triboelectric charge of the tribolayer more intuitively, as shown in Fig. 3c. The calculation method of TECD is: integrate I_{sc} to obtain the number of triboelectric charges, and then divide by the effective contact area of the tribolayer (16 cm^2), and finally obtain TECD. Unsurprisingly, the TECD of the two TENGs showed the same trend as that of I_{sc}. Compared with the cellulose acetate-based TENG, the TECD of the TESPN@CNF-based TENG was improved by 95%. Then, the triboelectric charge density (TECD) of CNF-based TENGs in the past five years was compared,[35–39] as shown in Fig. S6.† The TECD of the CNF-based green TENG is close to that of conventional polymers, which is a great improvement. Subsequently, the dependence of the I_{sc} and the corresponding power on the external loading resistance of these three TENGs was tested, as shown in Fig. S8.† When the resistance value was 50 MΩ, the cellulose acetate based TENG had a maximum output power of 0.85 mW, and the I_{sc} steadily decreases as the resistance increases. Similarly, the TESPN@CNF based TENG also exhibits the maximum output power when the load is 50 MΩ, but the value is increased to 3.64 mW.

In order to ensure a continuous and stable output of the green TENGs under real conditions, a stability test was performed, which is shown in Fig. 3d. After more than 10 000 cycles, the I_{sc} of the TESPN@CNF based TENG was stable at about 14.4 μA, indicating that the modified CNF based TENG can be stably used as an energy collecting device for a long time. In contrast, although the cellulose acetate based TENG also shows the stability of electrical output, the value of I_{sc} was low. In order to more clearly characterize the applicability of this TENG under realistic working conditions, a 51 hour durability experiment was performed, as shown in Fig. S7.† The results show that the I_{sc} of the TESPN@CNF-based TENG hardly drops during the 51.5 h test, which indicates that the TENG has excellent stability and is suitable as an energy harvester under realistic working conditions. Additionally, the real-time charges of cellulose acetate and TESPN@CNF films were tested by using a Faraday cup, as shown in Fig. 3e. In order to make sure that the charges on the surface of the films attained a saturated state, these two films were in contact-separated mode with the pure CNF film with the same impact force prior to the test. Then, each of the two charged films was quickly placed into the Faraday cup, and the electrical signal of the real-time charge change was captured by using a computer, as shown in Fig. S9.† The results show that the pure CNF film charged −5.5 nC and −19.4 nC for cellulose acetate and TESPN@CN films, respectively. The result of real-time charge is consistent with the calculated result of TECD, which is reasonable because both reflect the generation and dissipation of the surface triboelectric charges of the tribolayers during the contact electrification process. The more triboelectric charges, the stronger the triboelectric properties of the tribolayer.

In view of the stable and ultra-high electrical output performance of the TESPN@CNF based TENG, experiments to power LEDs were demonstrated. First, to demonstrate that the TESPN@CNF based TENG can successfully power the electrical appliances, the curves of it charging three capacitors with different capacities were collected, as shown in Fig. 3f. The results show that this TENG can charge capacitors of 2.2 μF, 4.7 μF and 10 μF with 10 V, 4.1 V and 2.2 V in 63 s, respectively. The circuit diagram of the TENG charging the capacitor is shown in the inset in Fig. 3f. Among them, the role of the rectifier is to convert the alternating current generated by the TENG into direct current. Based on this, the TESPN@CNF based TENG can easily light up 63 LEDs with patterned "TENG", as shown in the

digital photos in Fig. 3g and Video S1.† Moreover, the TENG can also power an electronic watch (Fig. 3h), showing its potential as a self-powered wearable device.

During the contact electrification process, the density of the transferred charges determines the electrical output of the TENG. However, the detrimental effect brought about by the rapid dissipation of triboelectric charges severely reduces the charge density of the tribolayer. As a result, the major aspects that influence the contact electrification effectiveness of polymer materials include the storage and dissipation of triboelectric charges at the friction interface. To investigate the effect of triboelectric charge dissipation on the triboelectrification of cellulose acetate and TESPN@CNF, the surface potentials of the two films were tested, as shown in Fig. 4a. Before the test, the cellulose acetate and TESPN@CNF films collided with the pure CNF film for one hour while being driven by a motor in order to reach a saturated state for the surface charge density. Then, the surface electrostatic tester quickly records the real-time surface potential. The results showed that the surface potential of the cellulose acetate film decreased from −142 V to −53 V within 115 s with a dissipation rate of 63%. However, the dissipation rate of the triboelectric charge of the TESPN@CNF film was reduced from −142 V to −86 V in the same time, and the reduction rate was only 39% (Fig. 4b).

For dielectric materials, the most common consequence of molecular self-assembly modification is a change in the dielectric properties, which leads to a change in the charge trapping/storage capacity of the material. In this study, the introduction of cyano-groups greatly enhanced the contact charging performance of CNF membranes. To explore the effect of the introduction of cyano-groups on the dielectric properties of the modified CNF films, the dielectric constant and capacitance of cellulose acetate and TESPN@CNF films were tested, as shown in Fig. 4c and d. To measure the dielectric constants, cellulose acetate and TESPN@CNF films were prepared on an Au/Si substrate, and Au as a top electrode was then deposited using an e-beam evaporator. For the cellulose acetate film, the dielectric constant was measured to be approximately 1.8 in the frequency range of 10^6–10^7 Hz, which is almost the same as in previous reports. However, the dielectric constant of the TESPN@CNF film reaches 2.5, an increase of 39%. Meanwhile, the capacitances of these two films were tested as shown in Fig. 4d. The results show that the capacitance of the TESPN film was increased by 26% compared with cellulose acetate in the range of 10^6–10^7 Hz, which is consistent with the change in the dielectric constant. The TESPN@CNF film's dielectric characteristics are enhanced by the addition of the cyano-group, which also lessens the dissipation of triboelectric charge into the environment. The improvement of the dielectric properties can enhance the injected charge density and internal capacitance of the TENG, thereby increasing the electrical output of the TENG. In addition, the dielectric losses of cellulose acetate and TESPN@CNF films were tested, as shown in Fig. S10.† The results show that the dielectric loss tangent values of all samples have no obvious change, which shows that the test results of the dielectric constant are quite reliable.[40] Another reason for the superior triboelectric performance of the TESPN@CNF film compared with cellulose acetate is the decrease of the crystallinity of CNF, which leads to more functional groups involved in triboelectrification. As shown in Fig. S11,† XRD of cellulose acetate and CNF was performed to calculate their crystallinity. The results show that the crystallinity of cellulose acetate is 59.1%, while that of CNF is only 41.5%, which was consistent with the expectation.

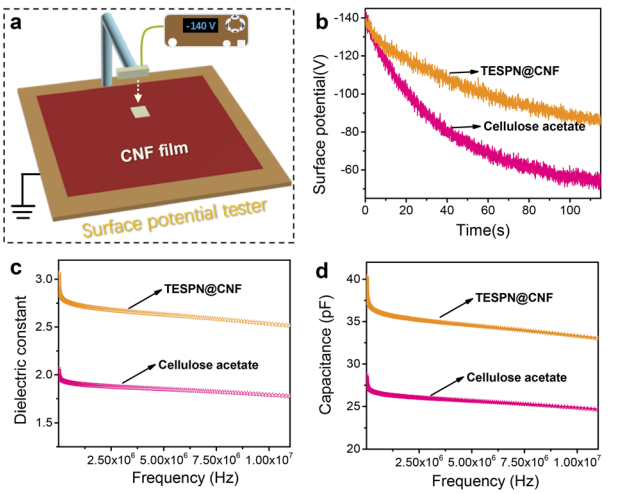

Fig. 4 (a) Schematic diagram of the surface charge test. (b) Surface charge *versus* time curves of cellulose acetate and TESPN@CNF films. Comparison of the (c) dielectric constant and (d) capacitance of cellulose acetate and TESPN@CNF films.

Given its ultra-high electric output performance, the TESPN@CNF-based TENG can be used as a wearable energy harvester for activity state sensing of human joints. When the human body moves, the flexion and extension of the joints provide the power source for the driving of the two tribolayers of the TENG. Fig. 5a shows the schematic diagram of the flexible and wearable TENG device. Pure CNF/Cu and TESPN@CNF/Cu constitute the positive and negative electrodes of the TENG, respectively. The schematic diagram of the sticking site of the TENG on body joints is shown in Fig. 5b. When the joint is flexed-extended, the two electrodes will contact-separate from each other to generate an electrical signal. At this time, the computer terminal connected to the electrode will receive a continuously changing electrical signal to prompt the change of the human body movement (Fig. 5c–f and Videos S2†), and then give an early warning of the body position, which has great application prospects in the field of recovery for trauma patients or guardianship of the elderly.

Benefiting from the ultra-high electrical output performance, the TESPN@CNF-based TENG can power small devices, such as self-powered power modules for cathodic protection systems. Fig. 6a shows the diagram of the TENG system for self-powered cathodic protection. The graphite electrode served as the connection for the rectified TENG device's positive pole, while A3 steel served as the connection for the device's negative pole. The current generated by the TENG device is rectified by the rectifier bridge and finally converted into direct current. After rectification, negative charges may flow from the rectifier bridge to the metal surface. Therefore, the TENG can prevent

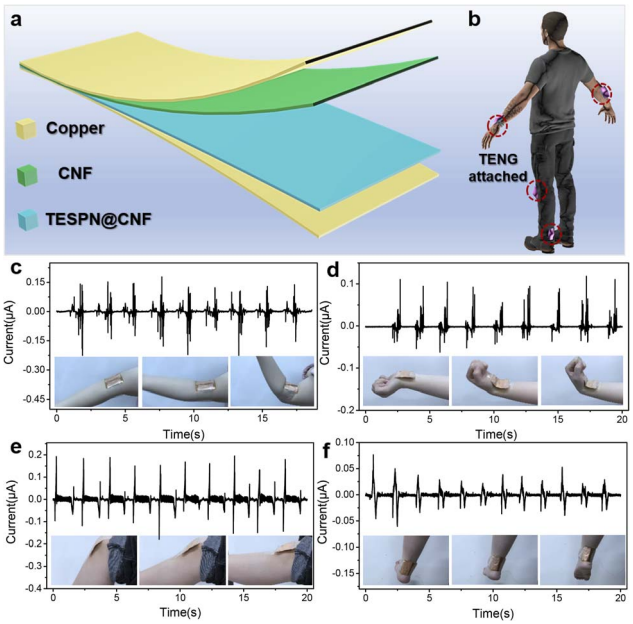

Fig. 5 (a) Schematic diagram of the flexible and wearable TENG. (b) Schematic diagram of the sticking site of the TENG on body joints. The electrical signals of the TENG attached to the (c) arm, (d) wrist, (e) knee and (f) ankle.

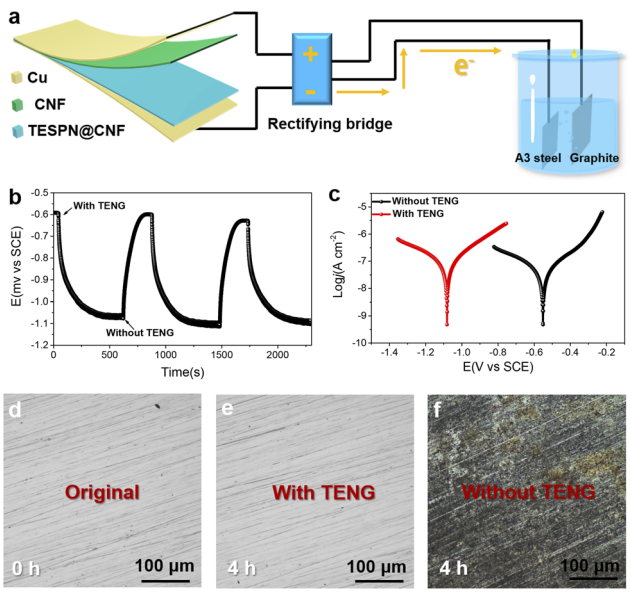

Fig. 6 (a) Diagram of the TENG system for self-powered cathodic protection. (b) OCP variants of A3 carbon steel coupled with and without the TENG. (c) Potentiodynamic polarization curves for the A3 carbon steel coupled with and without the TENG. (d–f) Optical images of A3 carbon steel after soaking in 3.5 wt% sodium chloride solution after 0 and 4 h when with and without the TENG.

the corrosion of A3 carbon steel in a marine environment. It is worth using the TENG device that connects and separates the OCP variant of A3 steel, where the reference and counter electrodes are saturated calomel electrodes (SCE) and platinum wires, respectively. The OCPs of the A3 steel that have been detached from the TENG device are still at −0.59 V, as seen in Fig. 6b. However, once linked to the TENG, the OCPs of the A3 steel exhibit a startling change (to −1.07 V) in a negative direction. The OCP drop value is 480 mV as a result, and the A3 steel may have efficient cathodic protection performance due to the obvious negative shift range. Additionally, the OCP rose to its starting amount when the A3 steel was unplugged from the TENG device. The consistency of the flexible TENG as the power supply for the ICCP system is validated by the repeatability of OCP fluctuation in the absence and presence of TENG connection.

The corresponding electrochemical tests were run to assess the cathodic protection system's ability to prevent corrosion when powered by the TENG. Fig. 6c displays the potentiodynamic polarization curves for A3 steel attached to and without the TENG device. The negative shift (−0.55 V to −1.08 V) of Ecorr in relation to cathodic protection by the TENG in this work shows that the friction electrons have moved to the steel in order to achieve cathodic protection. To verify the protection of the cathode metal by TENG power supply, two pieces of A3 steel with and without TENG power supply were placed in 3.5 wt% sodium chloride solution. The photos taken before and after the steel sheet was soaked in 3.5 wt% sodium chloride solution for 4 hours are shown in Fig. 6d–f. The improved TPU-based TENG gadget was propelled by a 10 ms^{-1} simulated natural wind in a humid atmosphere. The A3 steel sample that was used by the TENG did not exhibit any pitting characteristics. The black specks on A3 steel detached from the TENG clearly show pitting deterioration. The observed experimental phenomena suggest that the self-powered cathodic protection system may effectively cathodically guard A3 steel that has been submerged in a solution containing 3.5% NaCl.

4 Conclusions

In summary, we demonstrate a novel TESPN-modified CNF-based green TENG for mechanical energy harvesting. Benefiting from the electron-withdrawing effect of the cyano-group in TESPN, the modified CNF exhibits triboelectronegative. Furthermore, the electrical output of the CNF-TESPN@CNF-based TENG was enhanced by 95% compared with the commonly used electronegative cellulose acetate tribolayer. The decreased rate of triboelectric charge dissipation and enhanced charge storage performance are what account for the TESPN@CNF film's improved triboelectric performance. The modified CNF film's charge dissipation rate was 24% lower than that of cellulose acetate, according to the surface charge dissipation test. The accumulation of triboelectric charges on the surface of the tribolayer is further improved by the modified CNF film's higher dielectric constant. This type of TENG can serve as a self-powered power module, which has promising applications in wearable flexible electronics and cathodic protection.

Author contributions

Nannan Wang and Zibiao Li conceived the project idea. Yang Li, Sheng Wang and Bofan Li carried out the experiments. Enyi Ye

revised the manuscript. Nannan Wang, Xianjun Loh and Zibiao Li organized and wrote the manuscript with input from all authors.

Conflicts of interest

There are no conflicts to declare.

Acknowledgements

Thanks for the financial support of Zhongnan Hospital of Wuhan University, and Excellent Doctor Fund Project, China (Grant Number: ZNYB 2020012) for this work. N. Wang and Z. Li would also like to thank the financial support from the Agency for Science, Technology and Research (A*STAR), Science and Engineering Research Council (SERC) Central Research Fund (Use Inspired Basic Research).

Notes and references

1 N. Wang, Y. Liu, E. Ye, Z. Li and D. Wang, *Mater. Res. Lett.*, 2022, **10**, 97.
2 M. Li, H. Lu, S. Wang, R. Li, J. Chen, W. Chuang, F. Yang, Y. Lin, C. Chen and Y. Lai, *Nat. Commun.*, 2022, **13**, 1.
3 F. Fan, L. Lin, G. Zhu, W. Wu, R. Zhang and Z. L. Wang, *Nano Lett.*, 2012, **12**, 3109.
4 Y. Hu, M. Zhang, C. Qin, X. Qian, L. Zhang, J. Zhou and A. Lu, *Carbohydr. Polym.*, 2021, **265**, 118078.
5 J. Luo, W. Gao and Z. L. Wang, *Adv. Mater.*, 2021, **33**, 2004178.
6 W. Li, L. Lu, A. G. P. Kottapalli and Y. Pei, *Nano Energy*, 2022, 107018.
7 M. Zhou, M. Huang, H. Zhong, C. Xing, Y. An, R. Zhu, Z. Jia, H. Qu, S. Zhu and S. Liu, *Adv. Funct. Mater.*, 2022, 2200269.
8 S. Sriphan, U. Pharino, T. Charoonsuk, P. Pulphol, P. Pakawanit, O. Khamman, W. Vittayakom, N. Vittayakom and T. Maluangnont, *Nano Res.*, 2023, **16**, 3168.
9 B. Wang, Y. Wu, Y. Liu, Y. Zheng, Y. Liu, C. Xu, X. Kong, Y. Feng, X. Zhang and D. Wang, *ACS Appl. Mater. Interfaces*, 2020, **12**, 31351.
10 S. Fu, W. He, Q. Tang, Z. Wang, W. Liu, Q. Li, C. Shan, L. Long, C. Hu and H. Liu, *Adv. Mater.*, 2022, **34**, 2105882.
11 N. Wang, Y. Zheng, Y. Feng, F. Zhou and D. Wang, *Nano Energy*, 2020, 77, 105088.
12 C. Xing, Y. Tian, Z. Yu, Z. Li, B. Meng and Z. Peng, *ACS Appl. Mater. Interfaces*, 2022, **14**, 36741.
13 R. Wen, J. Guo, A. Yu, J. Zhai and Z. l. Wang, *Adv. Funct. Mater.*, 2019, **29**, 1807655.
14 Y. Wang, E. Yang, T. Chen, J. Wang, Z. Hu, J. Mi, X. Pan and M. Xu, *Nano Energy*, 2020, **78**, 105279.
15 N. Wang, Y. Liu, Y. Wu, Z. Li and D. Wang, *Nanoscale Adv.*, 2021, **3**, 6063.
16 W. Sun, N. Wang, J. Li, S. Xu, L. Song, Y. Liu and D. Wang, *Electrochim. Acta*, 2021, **391**, 138994.
17 N. Wang, Y. Feng, Y. Zheng, L. Zhang, M. Feng, X. Li, F. Zhou and D. Wang, *Adv. Funct. Mater.*, 2021, **31**, 2009172.
18 N. Wang, Y. Zheng, Y. Feng, L. Zhang, M. Feng, X. Li and D. Wang, *Front. Mater. Sci.*, 2021, **15**, 266.
19 X. Qu, X. Ma, B. Shi, H. Li, L. Zheng, C. Wang, Z. Liu, Y. Fan, X. Chen and Z. Li, *Adv. Funct. Mater.*, 2021, **31**, 2006612.
20 S. Nie, C. Cai, X. Lin, C. Zhang, Y. Lu, J. Mo and S. Wang, *ACS Sustainable Chem. Eng.*, 2020, **8**, 18678.
21 Y. Pang, F. Xi, J. Luo, G. Liu, T. Guo and C. Zhang, *RSC Adv.*, 2018, **8**, 6719.
22 Q. Zhou, J. Kim, K. Han, S. Oh, S. Umrao, E. J. Chae and I. Oh, *Nano Energy*, 2019, **59**, 120.
23 G. Liu, H. Guo, S. Xu, C. Hu and Z. L. Wang, *Adv. Energy Mater.*, 2019, **9**, 1900801.
24 X. Wu, X. Li, J. Ping and Y. Ying, *Nano Energy*, 2021, **90**, 106592.
25 S. Wang, P. Xu, X. Wang, J. Zheng, X. Liu, J. Liu, T. Chen, H. Wang, G. Xie and J. Tao, *Nano Energy*, 2022, 107210.
26 J. Zhang, Y. Li, J. Du, X. Hao and Q. Wang, *Nano Energy*, 2019, **61**, 486.
27 S. Nie, C. Cai, X. Lin, C. Zhang, Y. Lu, J. Mo and S. Wang, *ACS Sustainable Chem. Eng.*, 2020, **8**, 18678.
28 Y. Hu, X. Wang, H. Li, H. Li and Z. Li, *Nano Energy*, 2020, **71**, 104640.
29 S. Nie, Q. Fu, X. Lin, C. Zhang, Y. Lu and S. Wang, *Chem. Eng. J.*, 2021, **404**, 126512.
30 L. Liu, L. Zhou, C. Zhang, Z. Zhao, S. Li, X. Li, X. Yin, J. Wang and Z. L. Wang, *J. Mater. Chem. A*, 2021, **9**, 21357.
31 N. Wang, Y. Zheng, Y. Feng, F. Zhou and D. Wang, *Nano Energy*, 2020, **77**, 105088.
32 X. Ge, W. Zhang, F. Song, B. Xie, J. Li, J. Wang, X. Wang, J. Zhao and G. Cui, *Adv. Funct. Mater.*, 2022, 2200429.
33 K. Murali, S. Rajesh, O. Prakash, A. Kulkarni and R. Ratheesh, *Mater. Chem. Phys.*, 2009, **113**, 290.
34 N. Wang, W. Zhang, Z. Li, S. Wang, A. Suwardi, E. Ye, B. Li, Y. Liu, Z. Wu, Y. Dong, X. Loh and D. Wang, *Nano Energy*, 2022, **103**, 107748.
35 G. Khandelwal, T. Minocha, S. Yadav, A. Chandrasekhar, N. Raj, S. Gupta and S. Kim, *Nano Energy*, 2019, **65**, 104016.
36 J. Zhang, S. Hu, Z. Shi, Y. Wang, Y. Lei, J. Han, Y. Xiong, J. Sun, L. Zheng, Q. Sun, G. Yang and Z. Wang, *Nano Energy*, 2021, **89**, 106354.
37 Q. Zheng, Y. Zou, Y. Zhang, Z. Liu, B. Shi, X. Wang, Y. Jin, H. Ouyang, Z. Li and Z. Wang, *Sci. Adv.*, 2016, **2**, e1501478.
38 S. Hu, J. Han, Z. Shi, K. Chen, N. Xu, Y. Wang, R. Zheng, Y. Tao, Q. Sun, Z. Wang and G. Yang, *Micro Nano Lett.*, 2022, **14**, 115.
39 Z. Wang, C. Chen, L. Fang, B. Cao, X. Tu, R. Zhang, K. Dong, Y. Lai and P. Wang, *Nano Energy*, 2023, **107**, 108151.
40 J. Lee, H. Cho, J. Chun, K. Kim, S. Kim, C. Ahn, W. Kim, J. Kim, S. Kim, C. Yang and J. Baik, *Sci. Adv.*, 2017, **3**, e1602902.